ACUSTICA · acta acustica
Vol. 84 (1998) 432–447

Ultrasonic Separation of Suspended Particles - Part I: Fundamentals

Martin Gröschl
Institut für Allgemeine Physik, Technische Universität Wien, A-1040 Wien, Austria

Summary
Separation of suspended particles by means of acoustic forces is a promising alternative to conventional technologies. This paper concerns some of the latest developments of separation devices based on piezoelectric resonators. The acoustic forces on particles suspended in a liquid are reviewed. A mathematical model for the description of layered piezoelectric resonators is extended and applied to the calculation of the electrical properties and the acoustic field quantities of the resonator. A resonator for particle separation is analyzed and the optimum operating frequency range with respect to resonator efficiency (performance number) is determined. It is found that efficiency depends strongly on the frequency and the properties of the suspension. Results are in good agreement with experimental data and with a different approach based on perturbation theory.

PACS no. 43.35.Zc, 43.35.Bf

1. Introduction

Conventional processes for removing small suspended particles from a liquid are filtration, sedimentation, flocculation and centrifugation. The potential of separation techniques utilizing acoustic radiation pressure on suspended particles is known but has been relatively less developed. Nevertheless, there is a considerable body of literature on this topic and comprehensive review works have recently been published [1, 2, 3]. More recently, acoustic filters based on high-efficiency piezoelectric resonators have been developed primarily intended for mammalian cell separations in biotechnology applications [4, 5]. The main advantages of this novel type of acoustic separator are the absence of filter fouling, no need for moving parts, high separation efficiency and reliability. However, manufacturing cost are relatively high at this early stage and ultrasonic separation technology is still not used at a large scale. Possible applications in other fields, such as removing solid particles from liquids or splitting of emulsions, are currently being investigated.

The scope of this paper is to present the physical fundamentals of ultrasonic separation technology for utilizing piezoelectric resonators, with special emphasis on resonator analysis and optimization. In section 2, the acoustic forces on suspended spherical particles in liquids are reviewed. Section 3 is dedicated to the calculation of electrical properties and acoustic field quantities of the resonator, with the main objective being to obtain an expression for resonator efficiency (performance number). In section 4 the results are applied to the analysis of a resonator for particle separation.

This paper is the first in a series of three. In part II the design and operation of acoustic separation devices is treated with emphasis on electric power supply and resonance control. Part III describes in detail the first acoustic cell retention device, which has been introduced to the market recently.

Received 9 September 1996,
accepted 1 October 1997.

2. Acoustic forces on spherical particles in liquids

2.1. Primary radiation force in an ideal fluid

When a suspension is exposed to a sound field, the surrounding fluid exerts hydrodynamic forces on the suspended particles. In the linear approximation, these forces are proportional to the acoustic displacement velocity of the fluid [6] and, on the average, do not lead to a displacement of the particles. However, time-averaged forces that are related to the radiation pressure arise as a result of second order effects. King [7] derived the radiation pressure on a rigid sphere freely suspended in a non-viscous fluid by integrating the total sound pressure field (which is the sum of incident and scattered fields) over the surface of the object. Yosioka and Kawasima [8] extended the work of King to compressible spheres. Good agreement between theory and experiment was found. They obtained the following expressions for the mean radiation force in a plane progressive and a plane standing sound wave, respectively:

$$\left\langle F_p \right\rangle = 2\pi\rho\hat{\Phi}^2(ka)^6 K_p(\lambda,\sigma) = 4\pi k^4 a^6 \left\langle \bar{E}_p \right\rangle K_p(\lambda,\sigma), \tag{1}$$

$$\left\langle F_s(x) \right\rangle = 4\pi\rho\hat{\Phi}^2(ka)^3 K_s(\lambda,\sigma)\sin(2kx) = 4\pi ka^3 \left\langle \bar{E}_s \right\rangle K_s(\lambda,\sigma)\sin(2kx), \tag{2}$$

where a is the particle radius, $k = \omega/\nu$ is the wave number, and ρ is the density of the host fluid. $\hat{\Phi}$ denotes the amplitude of the velocity potential $\tilde{\Phi}$ of the incident sound wave, which is given by:

$$\tilde{\Phi}_p = \hat{\Phi}\,\mathrm{e}^{\mathrm{j}(\omega t - kx)}, \tag{3}$$

$$\tilde{\Phi}_s = \hat{\Phi}\left\{\mathrm{e}^{\mathrm{j}(\omega t - kx)} + \mathrm{e}^{\mathrm{j}(\omega t + kx)}\right\}. \tag{4}$$

It should be noted that in the original work [8] the term $\hat{\Phi}$ in equations (1) to (4) has been omitted. The acoustic contrast factors K_p and K_s take the form:

$$K_p(\lambda,\sigma) = \frac{1}{(1+2\lambda)^2}\left[\left(\lambda - \frac{1+2\lambda}{3\lambda\sigma^2}\right)^2 + \frac{2}{9}(1-\lambda)^2\right], \quad (5)$$

$$K_s(\lambda,\sigma) = \frac{1}{3}\left[\frac{5\lambda-2}{2\lambda+1} - \frac{1}{\lambda\sigma^2}\right]. \quad (6)$$

$\langle \bar{E}_p \rangle$ and $\langle \bar{E}_s \rangle$ are the time-averaged energy densities of the progressive and the standing wave, respectively:

$$\left\langle \bar{E}_p \right\rangle = \frac{1}{2}\rho k^2 \hat{\Phi}^2, \qquad \left\langle \bar{E}_s \right\rangle = \rho k^2 \hat{\Phi}^2. \quad (7)$$

Equations (1) and (2) hold in the limiting case: $ka \ll 1$, $k_0 a \ll 1$, $\lambda = O(1)$. That is, the particle radius must be small compared to the sound wavelength, and the particle and fluid densities have to be in the same order of magnitude. The authors [8] also present a general solution for arbitrary ka, $k_0 a$, and an expression for the radiation force on bubbles suspended in a liquid ($\lambda \ll 1$). For $\sigma \to \infty$, the acoustic contrast factors K_p and K_s reduce to the corresponding density factors for rigid spheres derived by King. As can be seen from equations (1-2), the radiation force in the progressive wave is of the order of $(ka)^6$ and herewith much smaller than the force in a standing wave, which is proportional to $(ka)^3$. This fact can be attributed to the different phase relations between the primary and scattered fields in a progressive and a standing wave, respectively [9]. While $\langle F_p \rangle$ is constant in space, $\langle F_s \rangle$ shows spatial dependence according to the factor $\sin(2kx)$. In a standing wave, particles collect at bands perpendicular to the direction of sound propagation, either at the velocity nodes or antinodes of the sound field, depending on the sign of the acoustic contrast factor. Because of this effect, which can be exploited in a number of ways, and due to the larger force amplitude, most practical concepts of particle separation rely on standing waves or moving "standing" waves, as will be discussed in part II of this work.

Gor'kov [10] used a different approach, based on principles of fluid dynamics, to express the radiation force F^G as the gradient of a radiation force potential ϕ^G:

$$\left\langle \phi^G(\boldsymbol{r}) \right\rangle = -V\left[\frac{3(\lambda-1)}{2\lambda+1}\left\langle \bar{E}_{kin}(\boldsymbol{r}) \right\rangle - \left(1 - \frac{1}{\lambda\sigma^2}\right)\left\langle \bar{E}_{pot}(\boldsymbol{r}) \right\rangle\right] \quad (8a)$$

$$\left\langle F^G(\boldsymbol{r}) \right\rangle = -\nabla\left\langle \phi^G(\boldsymbol{r}) \right\rangle, \quad (8b)$$

where $\boldsymbol{r} = (x, y, z)$ denotes the location of the particle and V is the particle volume. $\langle \bar{E}_{kin}(\boldsymbol{r}) \rangle$ and $\langle \bar{E}_{pot}(\boldsymbol{r}) \rangle$ are the time-averaged kinetic and potential energy densities, respectively, of the incident sound field at the point where the particle is located. Equations (8) are valid as long as the conditions

$$ka \ll 1, \qquad a \gg \delta = \sqrt{\frac{2\mu}{\rho\omega}}, \qquad a \gg \hat{u}, \quad (9)$$

hold. Here μ is the shear viscosity of the fluid and $\hat{u}$ is the displacement amplitude of the fluid particles in the sound wave. Equations (8) allow the radiation force to be calculated for an arbitrary sound field, except fields similar to a plane progressive wave (i.e. fields with low gradients of kinetic and potential energy densities). It can easily be verified that in case of a plane standing wave with $\langle \bar{E}_{kin}(x) \rangle = \langle \bar{E}_s \rangle \sin^2(kx)$ and $\langle \bar{E}_{pot}(x) \rangle = \langle \bar{E}_s \rangle \cos^2(kx)$ the expressions (8) and (2) lead to identical results. Based on the method developed by King, Nyborg [11] derived an expression for the radiation force (on rigid spheres) that corresponds to Gor'kov's (for $\sigma \to \infty$), but shows an additional additive term Δ, which dominates if the kinetic and potential energy densities of the sound field are essentially uniform (like in a plane traveling wave). For a standing wave, Δ is negligible. Equation (8a) can be used to calculate the radiation force potential in a resonator for particle separation, as will be shown in section 3.

Crum [12] investigated the acoustic radiation force in a standing wave on liquid droplets in theory and experiments. He showed that the total force can be expressed as the sum of the force that is obtained if the droplet is treated as a rigid sphere plus the force contribution due to its compressibility alone. His results agree with equation (2).

2.2. Secondary forces

So far, only the interaction (scattering) between a single particle and the incident (primary) sound field has been considered. When two objects are present in the sound field, the total incident field on one object includes the primary field and the scattered field of the other object. An acoustic interaction between the two objects results. This interaction effect was first investigated by König [13] who derived, based on Bernoulli's hydrodynamic principles, an expression for the force between two closely spaced spheres in an acoustic field. Later Bjerknes [14] calculated the attractive and repulsive forces between oscillating spheres, without considering the primary sound field. Thus, the acoustic interaction force is often called *Bjerknes* force but sometimes referred to as *König* force. Many other researchers also investigated the interaction of particles in a sound field [15, 16, 17]. Most of the studies, however, have been restricted to cases when the wavelength is much greater than the radii a and spacing d of the objects. In a recent work [18], Zheng and Apfel calculated the interaction force between two fluid spheres in a plane acoustic wave field without restriction on the particle spacing. Following in principle the method developed by Yosioka and Kawasima [8], the authors [18] expressed the total radiation force as the sum of the force due to the incident wave (equal to the primary radiation force) and the force due to the interaction effect. The latter reduces to the Bjerknes force in the case of $kd \ll 1$. In the approximation $ka \ll 1$, $kd \ll 1$, the interaction force between two identical compressible spheres in a plane standing wave was also calculated by Weiser [19]. Using the general result of Crum [12] allowing the superposition of rigid-sphere and compressibility contributions, he obtained for the interaction

ACUSTICA · acta acustica
Vol. 84 (1998)

force $\langle F_i(x)\rangle$:

$$\left\langle F_i(x)\right\rangle = 4\pi a^6\left\{\frac{(\rho_0-\rho)^2(3\cos^2\theta-1)}{6\rho d^4}v^2(x) - \frac{\omega^2\rho(\beta_0-\beta)^2}{9d^2}p^2(x)\right\}, \quad (10)$$

where d is the center-to-center distance of the spheres, β_0 and β are the compressibilities of the particles and the host fluid, respectively. θ is the angle between the centerline of the particles and the propagation direction of the incident sound wave; $v(x)$ and $p(x)$ are the velocity and pressure, respectively, of the unperturbed incident field at the position of the particles. In this approximation, it is assumed that $v(x) \simeq v(x+d)$ and $p(x) \simeq p(x+d)$. The first term on the right-hand side of equation (10) depends on the orientation of the particles with respect to the incident sound field. If the particles are lined up in the direction of sound propagation ($\theta = 0$), the first term represents a repulsive force contribution. If the centerline of the particles is oriented perpendicular to the traveling direction of the sound wave, the force contribution is attractive. The second term of equation (10) is independent of the particle orientation and represents an attractive force. The first term vanishes at the velocity nodes of the standing wave and does not act on particles that have been driven to the velocity nodes by the primary radiation force (like bubbles). Conversely, the second term vanishes at the pressure nodes (velocity antinodes) and therefore does not affect particles such as cells and solid particles, after they have been driven to the velocity antinodes by the primary radiation force. In general, the interaction force becomes significant only when the particles are very close to each other. In a plane standing wave, the interaction force will cause the particles to form clusters within the nodal or anti-nodal planes of the sound field. In special cases, the repulsive term may lead to a fine structure splitting of the bands, as has been observed for red blood cells by Weiser [19].

2.3. The effect of viscosity

The influence of fluid viscosity on the acoustic radiation pressure was first investigated by Westervelt [20]. He found that the radiation force exerted by a plane progressive wave on a rigid immobile sphere was vastly greater than that given by King's theory. The fluid viscosity effect arises due to losses within the boundary layer of the object and is particularly significant for small spheres and at low frequencies. An analysis carried out by Danilov [9] led to similar results for freely suspended particles in a progressive wave. Both works were restricted to small particles ($ka \ll 1$) and did not consider acoustic streaming. The most general treatment was presented in recent works by Doinikov [21, 22], who took the effect of acoustic streaming [23] into account. By solving the viscous equations of motion (Navier-Stokes equations) with a second order approximation, he obtained general solutions for the radiation force in a progressive and a standing wave, respectively, without restriction on particle size. Moreover, he distinguished between the influence of the viscosities μ of the host medium and μ_0 of the particle. Because of the complexity of the general solutions only the limiting case

$$ka \ll 1 \qquad k_0 a \ll 1 \qquad \mu \ll \rho\nu^2/\omega, \quad (11)$$

which is of interest for ultrasonic separation processes, will be discussed here. The last condition means that the sound wavelength is large compared to the penetration depth of the viscous wave ($k\delta \ll 1$) and therefore damping due to the viscosity of the host liquid is negligible. (Damping is considered in the derivation of the general solutions by the introduction of complex wave numbers.) Furthermore, one has to distinguish between two limiting cases:

a) $\mu \ll a^2\rho\omega$, $\mu_0 \ll a^2\rho_0\omega$:

In this low-viscosity approximation, the radiation force in a plane progressive wave is [22]:

$$\left\langle F_p^{vis}\right\rangle = 6\pi\rho\hat{\Phi}^2k^3a^2\delta\frac{(\lambda-1)^2}{(2\lambda+1)^2(1+\bar{\mu})}, \quad (12)$$

$$\text{with} \qquad \delta = \sqrt{\frac{2\mu}{\rho\omega}}, \qquad \bar{\mu} = \sqrt{\frac{\rho\mu}{\rho_0\mu_0}}.$$

Equation (12) is valid under the conditions $\lambda = O(1)$, $\bar{\mu} = O(1)$ (which is the interesting case here), or $\lambda \ll 1$, $\bar{\mu} \ll 1$. A comparison to equation (1) under consideration of $ka \ll 1$, shows that the radiation force in the viscous case can be several orders of magnitude higher than in the non- viscous case. On the other hand, this effect decreases rapidly with increasing frequency and particle size.

In a plane standing wave no significant change due to viscosity in this limiting case is found. Thus, the ratio between the radiation forces in standing and progressive waves, which is of the order of $(ka)^{-3}$ in the non-viscous case, decreases with increasing viscosity. However, a quantitative analysis shows that in most situations of practical interest the radiation force in a standing wave will remain much larger than the force in a progressive wave of comparable energy density. The results in the low-viscosity approximation discussed here are in good quantitative agreement with calculations carried out by Hager [24]. The second limiting case considered by Doinikov is:

b) $\mu \gg a^2\rho\omega$, $\mu_0 \gg a^2\rho_0\omega$:

whereby the relations (11) still hold. In this high-viscosity approximation, the radiation force in a plane standing wave can be expressed as [22]:

$$\left\langle F_s^{vis}(x)\right\rangle = 4\pi\rho\hat{\Phi}^2(ka)^3 \cdot G(\rho,\rho_0,\nu,\nu_0,\mu,\mu_0,a,\omega)\sin(2kx). \quad (13)$$

This result is very similar to equation (2), only the former acoustic contrast factor K_s is replaced here by a more complex expression G, which is a function of the fluid and particle properties as well as of frequency. For an explicit expression of G the reader is referred to [22]. The ratio G/K_s increases with increasing viscosity, but drops rapidly with increasing frequency and particle size. At high frequencies (in the

MHz-range) and for larger particles ($a \geq 1\,\mu$m), G/K_s may become negative, i.e. the direction of the radiation force changes. (Particles that are driven to the velocity antinodes in the non-viscous case are then driven to the velocity nodes and vice versa.) Moreover, under certain conditions the radiation force can become very small or even vanish. The ratio of the force amplitude in a standing wave and the force in a plane progressive wave may also drop below 1 under conditions of high viscosity. The expression for the latter is given in [22].

Many applications of ultrasonic separation (e.g., removing suspended particles from water, applications in biotechnology) may be well described by the low-viscosity limiting case (a) but in some situations (e.g., treatment of emulsions) conditions of high viscosity might have to be considered according to case (b). One reason for the increase of the radiation force due to viscosity is the development of acoustic streaming that leads to an additional drag force which contributes significantly to the radiation force, particularly in a progressive wave in the high- viscous case. According to Danilov [9] the influence of viscosity can be further explained as a change in the phase and amplitude relations between the primary and the scattered fields. In a progressive wave a significant change of the phase leads to an increase in the radiation force. This effect is particularly great at low frequencies and for heavy particles. In contrast, in a standing wave the viscosity causes an increase in the amplitude of the scattered field affecting the radiation force only to a much smaller extent. Danilov also showed that the secondary interaction force between particles is influenced by viscosity in a qualitatively similar way as the primary force.

2.4. Sound attenuation

In principle one has to distinguish between absorption in the particle and the host medium (host liquid). However, as long as the dimensions of the particles are small compared to the acoustic wavelength ($ka \ll 1$) and the volume fraction of particles is small, the sound absorption in the particles can be neglected. Hasegawa [25] investigated the influence of absorption of solid elastic spheres on the radiation force and showed that the effect becomes considerable in case of $ka \geq 1$. According to [26] the amplitude absorption coefficient α of liquids is given by:

$$\alpha = \frac{\omega^2}{2\rho\nu^3}\left(\mu' + \frac{4}{3}\mu\right). \tag{14}$$

Hence, absorption can be primarily attributed to viscous effects. Heat conduction is negligible in most cases. For water at room temperature ($\rho = 10^3\,\mathrm{kg/m^3}$, $\nu = 1500\,\mathrm{m/s}$, $\mu = 10^{-3}\,\mathrm{kg/ms}$, $\mu' = 2.4\,\mu$) the absorption coefficient according to equation (14) is $9 \cdot 10^{-2}\,\mathrm{m^{-1}}$ at a frequency of 2 MHz. Assuming a typical propagation length of the sound wave in a resonator chamber for particle separation of $\ell \leq 0.1$ m, the quantity $\mathrm{e}^{-\alpha\ell}$ is close to unity. Even for liquids of higher viscosity, neglecting absorption due to viscosity is justified, provided the sound frequency is not too high.

On the other hand, measurements of the electrical admittance spectra of piezoelectric resonators used for ultrasonic particle separation show clearly that in practice absorption due to other losses is significant. Measured resonance quality factors are typically in the range below 10^4. According to Auld [27], sound absorption can be described by an acoustic material quality factor Q, which is related to the absorption coefficient:

$$Q = \frac{k}{2\alpha}, \qquad (\text{for } Q \gg 1). \tag{15}$$

From the measured electrical admittance and resonance quality factors, an effective material quality factor Q_{eff} of the liquid (suspension) can be determined, as will be discussed in more detail in section 5. The effective quality factor provides an easy method to take into account additional losses like absorption of the sound wave due to gas bubbles in the liquid, divergence of the wave, absorption in the side walls, etc. The experimentally determined values of Q_{eff} for water at 2 MHz are typically in the range of 5000 to 10000 (depending on the resonator set-up), while the quality factor calculated from equations (14) and (15) is about 47000. The effective absorption (attenuation) coefficient α_{eff} of the liquid in the resonator can be regarded as the sum of the absorption coefficient α of the liquid alone and a second term $\bar{\alpha}$ representing additional losses:

$$\frac{k}{2Q_{eff}} = \alpha_{eff} = \alpha + \bar{\alpha}. \tag{16}$$

A more detailed analysis of viscous damping [27] shows a second order decrease of the wave number k and, consequently, a slight increase of the sound velocity ν compared to the undamped case. This effect is not considered here.

Due to attenuation, the sound wave in the resonator is a quasi-standing wave rather than a pure standing wave. A quasi-standing wave can be regarded as a superposition of two progressive waves with exponentially decreasing amplitudes traveling in opposite directions. Consider a one-dimensional attenuated plane wave originating at $x = 0$ and propagating in a medium 1 in x-direction. At position $x = \ell$ reflection at the boundary to a second medium with higher acoustic impedance is assumed. The superposition of incident and reflected waves can be expressed by the complex displacement function

$$\begin{aligned}\tilde{u}(x,t) &= \hat{u}\left\{\mathrm{e}^{-\alpha x}\mathrm{e}^{\mathrm{j}(\omega t - kx)} - R\cdot\mathrm{e}^{-\alpha(2\ell - x)}\mathrm{e}^{\mathrm{j}(\omega t + kx)}\right\} \\ &= \tilde{u}(x)\cdot\mathrm{e}^{\mathrm{j}\omega t},\end{aligned} \tag{17a}$$

with

$$\tilde{u}(x) = \hat{u}\left\{\mathrm{e}^{-\alpha x}\mathrm{e}^{-\mathrm{j}kx} - R\cdot\mathrm{e}^{-\alpha(2\ell - x)}\mathrm{e}^{\mathrm{j}kx}\right\}, \tag{17b}$$

where $\hat{u}$ denotes the amplitude of the positive-traveling wave at $x = 0$ and R is the reflection coefficient ($0 \leq R \leq 1$). For clarity, the subscript "*eff*" of the absorption coefficient a has been omitted. Equation (17) is valid for $k\ell = n \cdot 2\pi$

ACUSTICA · acta acustica
Vol. 84 (1998)

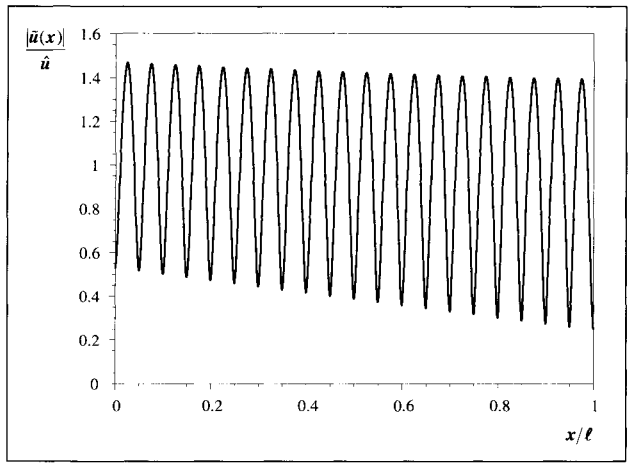

Figure 1. Plot of the normalized displacement amplitude of a quasi-standing wave according to equation (17), with $\alpha\ell = 0.2$, $k\ell = 20\pi$, and $R = 0.7$.

($n = 1, 2, 3 \ldots$). Absorption within the medium is described by the condition $\alpha > 0$, as discussed before, while the condition $R < 1$ accounts for absorption in the reflective wall at $x = \ell$. In Figure 1 the spatial progress of the (normalized) displacement amplitude of an attenuated quasi-standing wave according to equation (17) is shown.

To calculate the radiation force in the quasi-standing wave by use of equations (8) one has to insert the corresponding expressions for the gradients of the kinetic and potential energy densities. With the general expressions

$$\left\langle \bar{E}_{kin}(x) \right\rangle = \frac{1}{2}\rho \left\langle v^2(x) \right\rangle, \tag{18a}$$

$$\left\langle \bar{E}_{pot}(x) \right\rangle = \frac{1}{2\rho\nu^2} \left\langle p^2(x) \right\rangle, \tag{18b}$$

and the linear equation of motion

$$-\frac{\partial p(x,t)}{\partial x} = \rho \frac{\partial^2 u(x,t)}{\partial t^2} = \rho \frac{\partial v(x,t)}{\partial t} \tag{19}$$

one obtains with equation (17) and $u(x,t) = \Re\{\tilde{u}(x,t)\}$, the energy density gradients as:

$$\frac{d}{dx}\left\langle \bar{E}_{kin}(x) \right\rangle = \rho k^3 \hat{\Phi}\hat{\Phi}' \mathrm{e}^{-2\alpha\ell} \sin(2kx), \tag{20a}$$

$$\frac{d}{dx}\left\langle \bar{E}_{pot}(x) \right\rangle = -\rho k^3 \hat{\Phi}\hat{\Phi}' \mathrm{e}^{-2\alpha\ell} \sin(2kx), \tag{20b}$$

where $\hat{\Phi} = \hat{u}\omega/k$, $\hat{\Phi}' = \hat{u}R\omega/k$. Equations (20) are valid as long as

$$Q = \frac{k}{2\alpha} \gg k\ell, \quad \alpha \ll \frac{1}{2\ell}, \quad \frac{\hat{\Phi}'}{\hat{\Phi}} \gg \frac{1}{2k\ell}. \tag{21}$$

With equations (8) and (20) the radiation force in the attenuated quasi-standing wave turns out to be:

$$\left\langle F_{qs}(x) \right\rangle = 4\pi\rho\hat{\Phi}\hat{\Phi}'(ka)^3 \mathrm{e}^{-2\alpha\ell} \cdot \frac{1}{3}\left[\frac{5\lambda - 2}{(2\lambda + 1)} - \frac{1}{\lambda\sigma^2}\right] \sin(2kx). \tag{22}$$

Equation (22) indicates that the amplitude of the radiation force in a quasi-standing wave in cases of low damping remains constant in space but is reduced by the factor $(\hat{\Phi}'/\hat{\Phi})\mathrm{e}^{-2\alpha\ell}$, compared with equation (2) for the ideal standing wave. Hasegawa [28] calculated the primary radiation force $\langle F_{qs}(x)\rangle$ for an undamped quasi-standing plane wave in an ideal fluid. Considering a velocity potential of the form

$$\tilde{\Phi}_{qs} = \hat{\Phi}\mathrm{e}^{\mathrm{j}(\omega t - kx)} + \hat{\Phi}'\mathrm{e}^{\mathrm{j}(\omega t + kx)} \tag{23}$$

with $\hat{\Phi}' \leq \hat{\Phi}$, and using the same approach as for derivation of equations (1) and (2) he obtained:/

$$\left\langle F_{qs}(x) \right\rangle = \left[1 - \left(\frac{\hat{\Phi}'}{\hat{\Phi}}\right)^2\right] \left\langle F_p \right\rangle + \frac{\hat{\Phi}'}{\hat{\Phi}} \left\langle F_s(x) \right\rangle, \tag{24}$$

whereby $\langle F_p \rangle$ and $\langle F_s(x)\rangle$ are given by equations (1) and (2), respectively. Since in most practical cases $\langle F_p \rangle$ is several orders of magnitude smaller than the amplitude of $\langle F_s(x)\rangle$, the radiation force in the quasi-standing wave is dominated by the contribution of the standing wave, even in case of low standing wave ratio ($\hat{\Phi}' \ll \hat{\Phi}$), and may therefore be approximated by:

$$\left\langle F_{qs}(x) \right\rangle \cong 4\pi\rho\hat{\Phi}\hat{\Phi}'(ka)^3 K_s(\lambda, \sigma) \sin(2kx). \tag{25}$$

Taking attenuation into account by substituting space-dependent amplitudes

$$\hat{\Phi} \to \hat{\Phi}\mathrm{e}^{-\alpha x}, \qquad \hat{\Phi}' \to \hat{\Phi}'\mathrm{e}^{-\alpha(2\ell - x)}, \tag{26}$$

into equation (25), leads to the same result as given by equation (22). This procedure is justified since the amplitudes can be regarded to be constant for integration over the particle surface. It should be noted, that the velocity potential according to equation (23) modified by equation (26) represents correctly the displacement function (17) only if the condition $\alpha \ll k$ is satisfied. Neglecting the contribution of the progressive part of the quasi-standing wave by use of equation (22) or (25), does not lead to significant errors in cases of sufficiently high standing wave ratio and low damping.

2.5. Consideration of real field geometry

Only plane waves have been considered in the above discussion of acoustic forces. In a real resonator the sound field will have amplitude variations not only in the direction of wave propagation but also in lateral directions. This can be caused by non-uniform amplitude distribution of the source, divergence of the wave, influence of the boundaries, etc. In acoustic fields with lateral energy gradients additional forces on suspended particles arise, as can be seen from equations (8). Let us consider a standing wave propagating in x-direction, having a lateral amplitude distribution function $u_s(y)$:

$$u(x, y, t) = u_s(y) \sin(kx) \sin(\omega t). \tag{27}$$

According to equations (8), this leads to a lateral force acting in the positive y-direction, given by:

$$\left\langle F_y(x,y)\right\rangle = \frac{2\pi}{3}\rho\omega^2 a^3 u_s(y)\frac{\mathrm{d}u_s(y)}{\mathrm{d}y} \cdot \left[\frac{3(\lambda-1)}{2\lambda+1}\sin^2(kx) - \left(1-\frac{1}{\lambda\sigma^2}\right)\cos^2(kx)\right]. \tag{28}$$

Assuming a constant amplitude gradient in the vicinity of a small spherical particle with radius a, the function $u_s(y)$ may be written as:

$$u_s(y) = \hat{u}_0 + \frac{\hat{u}_m}{a}y, \tag{29}$$

where $\hat{u}_0$ denotes the displacement amplitude of the sound wave at the center of the particle (which is assumed to be at position $y = 0$) and $\hat{u}_0 + \hat{u}_m$ is the amplitude at the surface of the particle at $y = a$. For dense particles ($\lambda \gg 1$), the lateral force at the velocity antinodes, i.e. at positions $kx = (2n+1)\pi/2$ ($n = 0, 1, 2\ldots$), can be approximated by:

$$\left\langle F_y\right\rangle = \pi\rho\omega^2 a^2 \hat{u}_0 \hat{u}_m. \tag{30}$$

Equation (30) corresponds to a result presented by Benes [29], obtained by a different approach. The lateral force is sometimes referred to as *Bernoulli* force. Particles, which form bands at the velocity antinodes of the sound field due to the primary radiation force $\langle F_s\rangle$, are further driven to regions of relative amplitude maxima within these bands due to the lateral force $\langle F_y\rangle$. Hence, the particles form "striated" columns in the direction of sound propagation. Most types of suspended particles will be driven to regions of amplitude maxima (e.g., to the center of a cylindrical wave guide with a Gaussian-shaped amplitude distribution). But in certain situations (e.g., particles that are less dense and less compressible than the host liquid) the lateral forces will drive the particles towards locations of amplitude minima (e.g., to the walls of a wave guide). This effect has been studied in detail by Whitworth [30]. For particle separation, the preferred lateral amplitude distribution may be uniform, Gaussian-shaped, or periodically varying, depending on whether lateral forces are utilized in the separation process, or not. Various types of separation systems will be discussed in part II of this work.

3. One-dimensional mathematical model for layered piezoelectric resonators

In this section, a resonator for the generation of a standing ultrasonic field in a liquid suspension is investigated. Such a resonator typically consists of 4 layers, a piezoceramic transducer, a glass carrier isolating the piezoceramic from the liquid, the suspension, and a reflector (Figure 2). Mathematical models for the description of piezoelectric structures have been based on electro-acoustic equivalent circuits [31, 32], a transmission line model [33, 34], or a transfer matrix approach [35, 36, 37]. The analysis in this work follows the one-dimensional transfer matrix model of Nowotny [38]. All considered quantities are assumed to show space-dependence in only one direction, that is the direction of sound propagation (thickness direction of the layers). Furthermore, the displacement of the sound wave is restricted to this direction. This treatment is justified, because the considered piezoceramic disc transducers allow electrical excitation in only the thickness direction.

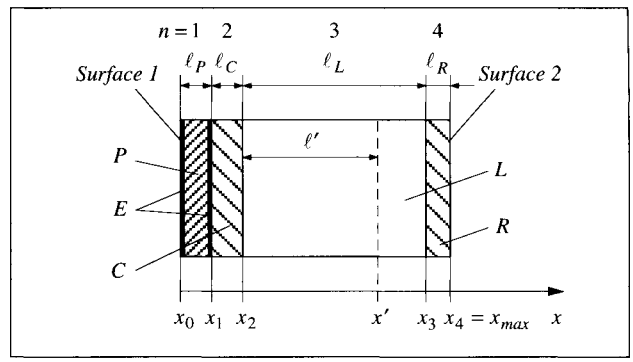

Figure 2. Piezoelectric resonator comprising one active (piezoceramic) and three passive layers; sound propagates in x-direction. P: piezoceramic, E: electrodes, C: carrier (glass), L: liquid (suspension), R: reflector (glass).

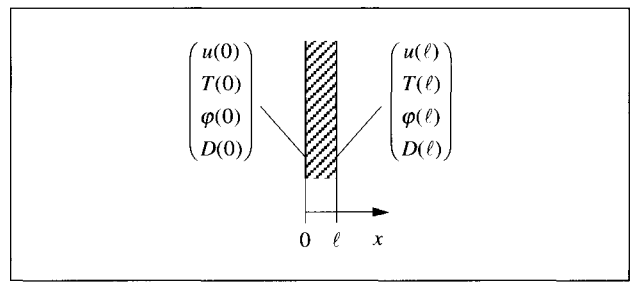

Figure 3. Piezoelectric layer of thickness ℓ; boundary values of u, T, φ, and D, at $x = \ell$, are calculated from the corresponding values at $x = 0$.

3.1. Calculation of electrical admittance

In the linear theory of piezoelectricity, for the quasi-static electric approximation, the coupled electromagnetic and acoustic fields in a lossless piezoelectric medium can be described by displacement u, stress T, electric potential φ, and dielectric displacement D. These field quantities are related by the fundamental equations [27]:

$$T = c\frac{du}{dx} + e\frac{d\varphi}{dx}, \tag{31}$$

$$D = e\frac{du}{dx} - \varepsilon\frac{d\varphi}{dx}, \tag{32}$$

where c, e, ε, are the elastic stiffness constant, piezoelectric constant, and dielectric constant, respectively, of the medium. As a consequence of the restriction to a single displacement direction, all material constants, which are tensor quantities in the general case, are reduced to the scalar quantities that

ACUSTICA · acta acustica
Vol. 84 (1998)

apply to the direction of sound propagation. For a single homogeneous piezoelectric layer of thickness ℓ (Figure 3), in case of harmonic time-dependence, the boundary values $u(\ell)$, $T(\ell)$, $\varphi(\ell)$, $D(\ell)$, can be calculated from the corresponding values at $x = 0$ using a matrix notation:

$$\begin{pmatrix} u \\ T \\ \varphi \\ D \end{pmatrix}_{x=\ell} = \boldsymbol{M} \begin{pmatrix} u \\ T \\ \varphi \\ D \end{pmatrix}_{x=0},$$

with

$$\boldsymbol{M} = \begin{pmatrix} M^{uu} & M^{uT} & M^{u\varphi} & M^{uD} \\ M^{Tu} & M^{TT} & M^{T\varphi} & M^{TD} \\ M^{\varphi u} & M^{\varphi T} & M^{\varphi\varphi} & M^{\varphi D} \\ M^{Du} & M^{DT} & M^{D\varphi} & M^{DD} \end{pmatrix}. \quad (33)$$

The elements of the transfer matrix $\boldsymbol{M}$ depend only on the material constants ρ, c, e, ε, the layer thickness ℓ, and the angular frequency ω. The explicit expressions for the matrix elements M^{ii} were given by Nowotny [38]. For multiple layers, the total transfer matrix $\boldsymbol{M}_{tot}$ of the layered structure can be obtained by multiplication of the transfer matrices of each single layer. This follows from the continuity condition that applies to u, T, and φ at the interfacing surfaces. The dielectric displacement D shows continuity only if there is no electrode between the considered layers. Each electrode is treated as a separate layer and represented by a transfer matrix $\boldsymbol{M}_E$. For the structure shown in Figure 2, the total transfer matrix is given by:

$$\boldsymbol{M}_{tot} = \boldsymbol{M}_E \cdot \boldsymbol{M}_P \cdot \boldsymbol{M}_E \cdot \boldsymbol{M}_C \cdot \boldsymbol{M}_L \cdot \boldsymbol{M}_R. \quad (34)$$

$\boldsymbol{M}_E$ relates the dielectric displacement D with the electric current I in the electrode and is a function of the electrical admittance Y between the two electrodes and of the electrode area A. Since in the structure of Figure 2 there is no electric field in the non-piezoelectric layers C, L, and R, the transfer matrices $\boldsymbol{M}_C$, $\boldsymbol{M}_L$, $\boldsymbol{M}_R$, depend only on ρ, c, and ℓ of the corresponding layers, and on ω.

On the outer free surfaces 1 and 2 of the total sandwich arrangement, stress and dielectric displacement are zero:

$$T = 0, \quad D = 0, \quad \text{for } x = \begin{cases} x_0 \\ x_{max} \end{cases}. \quad (35)$$

The relation between the boundary values on these surfaces can therefore be written in the form:

$$\begin{pmatrix} u_2 \\ 0 \\ \varphi_2 \\ 0 \end{pmatrix}_{x=x_{max}} = \boldsymbol{M}_{tot} \begin{pmatrix} u_1 \\ 0 \\ \varphi_1 \\ 0 \end{pmatrix}_{x=x_0}, \quad (36)$$

where values at surface 1 have been indicated with subscript "1" and values at surface 2 with subscript "2". With the general form of $\boldsymbol{M}$ given in equation (33) it follows from (36) that

$$0 = M^{Tu} u_1 + M^{T\varphi} \varphi_1, \quad (37)$$

$$0 = M^{Du} u_1 + M^{D\varphi} \varphi_1. \quad (38)$$

From equation (37) one obtains a relation between the displacement and the electric potential on the outer surface 1 (outer electrode) of the layered structure:

$$u_1 = -\left(M^{Tu}\right)^{-1} M^{T\varphi} \varphi_1. \quad (39)$$

Furthermore, an expression for the electrical admittance Y of the resonator as a function of the angular frequency ω can be derived from equations (37) and (38). This result, which is explicitely given in [38], and equations (33) and (39) are the basis for further resonator analysis in sections 3.3 and 3.4.

As discussed in section 2.5, a real acoustic transducer has a non-uniform lateral amplitude distribution. This fact can be taken into account globally in the one-dimensional model either by use of an equivalent area (smaller than the cross-sectional area A of the resonator) [39], or by a reduced (effective) coupling factor of the piezoelectric disc. The first approach is especially suitable for Gaussian-type transducers. The electromechanical coupling factor is defined as the square root of the ratio of available mechanical (acoustic) energy and supplied electric energy. For an ideal (one-dimensional) thickness vibration, the electromechanical coupling factor κ is given by

$$\kappa = \frac{e}{\sqrt{\bar{c}\varepsilon}}, \quad (40)$$

with the piezoelectrically stiffened elastic constant $\bar{c} = c + e^2/\varepsilon$ [40], elastic stiffness constant c, piezoelectric constant e, and dielectric constant ε, effective in direction of sound propagation. A reduced coupling factor of the piezoelectric disc accounts for energy loss due to parasitic oscillations (e.g., radial modes) that can occur in a transducer with finite lateral dimensions. As will be shown in section 4, good agreement between measured and calculated electrical admittance spectra is achieved by use of the one-dimensional description presented here. The mathematical model is also applicable to layered structures with an arbitrary number of electrodes [41].

3.2. Consideration of losses

The discussion in the previous section did not consider losses. However, losses can be accounted for in an elegant way, as will be shown in this section. In the absence of an electric field equation (31) corresponds to Hooke's law, which relates stress T and strain S:

$$T = cS. \quad (41)$$

Following Auld [27], equation (41) can be modified to include viscoelastic damping by adding a term that contains the time derivative of the strain:

$$T = cS + \mu \frac{\partial S}{\partial t}. \quad (42)$$

For a harmonic time dependence $e^{j\omega t}$ of the acoustic field, equation (42) can be written in complex notation as

$$\tilde{T} = c\tilde{S} + j\omega\mu\tilde{S} = \tilde{c}\tilde{S}, \quad (43)$$

where the complex elastic stiffness constant

$$\tilde{c} = c + \mathrm{j}\omega\mu \tag{44}$$

has been introduced. As already discussed in section 2.4, damping by a medium can be characterized by the acoustic material quality factor Q defined as:

$$Q = \frac{c}{\omega\mu}. \tag{45}$$

The definition (45) is compatible with equation (15), as shown in [27]. For a liquid, μ has to be replaced by the total viscosity coefficient: $\mu \to \mu + \mu'$. With (45), equation (44) takes the form:

$$\tilde{c} = c\left(1 + \mathrm{j}\frac{1}{Q}\right). \tag{46}$$

According to the relation between sound velocity and the stiffness constant, $\nu = \sqrt{\tilde{c}/\rho}$, complex notation leads to a complex sound velocity, which for $Q \gg 1$ is given by:

$$\tilde{\nu} = \nu\left(1 + \mathrm{j}\frac{1}{2Q}\right). \tag{47}$$

Damping due to dielectric losses can be accounted for by adding an imaginary part to the dielectric constant [42, 43]:

$$\tilde{\varepsilon} = \varepsilon + \frac{\gamma}{\mathrm{j}\omega} \tag{48}$$

where γ is the electric conductivity. For a large plate of constant thickness, γ can be expressed as $\gamma = \omega\varepsilon\tan\vartheta$. Hence, equation (48) becomes:

$$\tilde{\varepsilon} = \varepsilon\,(1 - \mathrm{j}\tan\vartheta)\,. \tag{49}$$

The dielectric loss angle ϑ is usually specified by the manufacturer of piezoelectric transducers. A third loss mechanism, piezoelectric loss, can be neglected in most practical cases and is not considered here.

The concept of complex material constants allows all calculations to be carried out in exactly the same way as for the lossless case, except that complex notation must be used. Thus, damping can be considered in a straight-forward way. As already discussed earlier, additional losses (besides viscoelastic damping) can be represented by use of effective quality factors instead of the values given by equations (14) and (15) or (45). In principle, the imaginary parts of the material constants are frequency-dependent. However, if the frequency range considered is limited, they can to close approximation be treated as constants. While the frequency-dependence of the viscoelastic damping mechanism is well defined, it is hard to predict for other losses. Thus, the dependence on frequency of the effective quality factor would need to be determined experimentally.

3.3. Calculation of acoustic field quantities within the layers

According to the method outlined in the previous section, complex material constants will be used in the following calculations to account for losses. As a consequence, the elements of the transfer matrices and the acoustic and electric field quantities introduced in section 3.1 become complex, too. Given the values of $\tilde{u}$, $\tilde{T}$, $\tilde{\varphi}$, $\tilde{D}$, at one boundary surface ($x = 0$) of a layer, the corresponding values at the opposite boundary surface ($x = \ell$) can be calculated from equation (33). Furthermore, the matrix method allows calculation of the spatial dependence of the considered quantities within the layer. This calculation is performed for a selected frequency ω. In the first step, the electrical admittance $\tilde{Y}(\omega)$ of the multilayer arrangement is computed. (This is needed for calculation of the transfer matrices $\boldsymbol{M}_E$ of the electrodes.) Subsequently, the acoustic field quantities are calculated at positions $x = x'$ (with x' running from x_0 to x_{max}) by stepwise evaluation of the transfer matrix $\boldsymbol{M}_n$ of the corresponding layer, whereby the layer thickness ℓ is replaced by the variable thickness $\ell' = x' - x_{n-1}$ of the sub-layer (Figure 2):

$$\begin{pmatrix} \tilde{u} \\ \tilde{T} \\ \tilde{\varphi} \\ \tilde{D} \end{pmatrix}_{x=x'} = \boldsymbol{M}_n(x' - x_{n-1}) \begin{pmatrix} \tilde{u} \\ \tilde{T} \\ \tilde{\varphi} \\ \tilde{D} \end{pmatrix}_{x=x_{n-1}}. \tag{50}$$

Since the (thin) electrode layers can be treated as massless, they do not influence the progress of displacement $\tilde{u}$ and stress $\tilde{T}$. The transfer matrices of the piezoelectric layer and the electrodes can be combined to a total transfer matrix $\boldsymbol{M}_1$ of the active layer: $\boldsymbol{M}_1 = \boldsymbol{M}_E\boldsymbol{M}_P\boldsymbol{M}_E$. The initial values at free surface 1 ($x = x_0$) are:

$$\begin{aligned} &\tilde{u}_1, \qquad \tilde{T}_1 = 0, \qquad \Re\{\tilde{\varphi}_1\} = \hat{U}, \\ &\Im\{\tilde{\varphi}_1\} = 0, \qquad \tilde{D}_1 = 0, \end{aligned} \tag{51}$$

where $\hat{U}$ denotes the amplitude of the driving voltage ($\tilde{\varphi}_2$ is chosen to be zero). The initial displacement $\tilde{u}_1$ is calculated from the complex equivalent of equation (39). With this procedure, one obtains (with chosen resolution) the discrete spatial distributions of $\tilde{u}(x)$, $\tilde{T}(x)$, $\tilde{\varphi}(x)$, and $\tilde{D}(x)$. From these primary quantities, other interesting quantities can be easily derived. The displacement velocity in complex notation is calculated from

$$\tilde{v}(x) = \mathrm{j}\omega\tilde{u}(x). \tag{52}$$

According to Poynting's theorem for piezoelectric media, in the one-dimensional case the Poynting vector in complex notation is given by:

$$\tilde{\Pi}(x) = \frac{1}{2}\left[-\tilde{v}^*(x)\,\tilde{T}(x) + \tilde{\varphi}(x)\,\left(\mathrm{j}\omega\,\tilde{D}(x)\right)^*\right]. \tag{53}$$

The asterisk denotes complex conjugation. Equation (53) can be derived directly from Maxwell's equations [27]. The real part of (53) represents true energy flow density (in W/m^2) and

ACUSTICA · acta acustica
Vol. 84 (1998)

is therefore a time-averaged quantity. The imaginary part is peak reactive energy flow density. (The time-average of reactive energy flow is zero.) Positive sign of the Poynting vector means energy flow in positive x-direction. Furthermore, the mean total stored energy density (J/m^3) can be calculated from:

$$\left\langle \bar{E}(x) \right\rangle = \frac{1}{4}\left[\rho\tilde{v}(x)\,\tilde{v}^*(x) + \Re\left\{\tilde{T}(x)\,\tilde{S}^*(x) - \frac{\mathrm{d}\tilde{\varphi}}{\mathrm{d}x}\tilde{D}^*(x)\right\}\right], \tag{54}$$

where $\mathrm{d}\tilde{\varphi}/\mathrm{d}x$ can be obtained from equations (31) and (32). The first term on the right-hand side of equation (54) is the kinetic energy density. In a piezoelectric material, the second and third terms are neither purely mechanical nor purely electrical, since they represent the piezoelectric coupling described by equations (31) and (32).

Following from Poynting's theorem, the averaged power loss density (W/m^3) can be derived as [27]:

$$\left\langle \bar{P}^{loss}(x) \right\rangle = \frac{1}{2}\omega \cdot \Im\left\{\tilde{T}(x)\,\tilde{S}^*(x) - \frac{\mathrm{d}\tilde{\varphi}}{\mathrm{d}x}\tilde{D}^*(x)\right\}. \tag{55}$$

If there is no electric field in the passive (non-piezoelectric) layers, as in the structure considered here, equations (50) and (53) to (55) can be simplified (for the passive layers), since $\tilde{\varphi} = 0$, $\tilde{D} = 0$. Equation (53) then represents pure mechanical energy flow density. The remaining terms of equation (54) represent mean kinetic and potential energy density, respectively:

$$\begin{aligned}\left\langle \bar{E}(x) \right\rangle &= \left\langle \bar{E}_{kin}(x) \right\rangle + \left\langle \bar{E}_{pot}(x) \right\rangle \\ &= \frac{1}{4}\left[\rho\tilde{v}(x)\,\tilde{v}^*(x) + \Re\left\{\tilde{T}(x)\,\tilde{S}^*(x)\right\}\right].\end{aligned} \tag{56}$$

Using equation (56) the acoustic radiation force potential in the liquid layer of the piezoelectric resonator can be calculated from equation (8a).

3.4. Calculation of resonator performance numbers

Knowledge of the distribution of stored energy and power loss among the layers is essential for the development of practical resonators. This distribution depends strongly on the frequency as well as on the resonator construction (material properties, thickness of the layers) and on the properties of the suspension. To determine the optimum driving frequency for a given layered resonator, the acoustic performance number η_{ac} is defined here as:

$$\eta_{ac} = \frac{\left\langle E_L \right\rangle}{\left\langle E_{tot}^{loss} \right\rangle} = \frac{\omega}{2\pi} \cdot \frac{\left\langle E_L \right\rangle}{P_{el}^{true}}, \tag{57}$$

where $\langle E_L \rangle$ is the stored energy in the liquid layer and $\langle E_{tot}^{loss} \rangle$ is the total energy loss in the resonator averaged over one oscillation period. Since the entire energy is supplied by an electric driving source, $\langle E_{tot}^{loss} \rangle$ must be equal to the electric true energy consumption per period, which in turn is given by the true electrical input power P_{el}^{true} divided by the oscillation frequency. Further, the effective performance number η_{eff} of the resonator is defined here as:

$$\eta_{eff} = \frac{\omega}{2\pi} \cdot \frac{\left\langle E_L \right\rangle}{P_{el}^{app}}, \tag{58}$$

with P_{el}^{app} being the apparent electrical input power supplied by the source. The stored energy in the liquid can be calculated from the energy density given by equation (56) as:

$$\left\langle E_L \right\rangle = A \int_{x=x_2}^{x=x_3} \left\langle \bar{E}(x) \right\rangle \mathrm{d}x, \tag{59}$$

where x_2, x_3 define the boundaries of the liquid layer as shown in Figure 2 and A is the active cross-sectional area of the resonator (electrode area of the piezoceramic). For computation purposes the integration is approximated by a summation. P_{el}^{true} and P_{el}^{app} are given by

$$P_{el}^{true} = \frac{1}{2}\hat{U}^2 \Re\left\{\tilde{Y}\right\} \tag{60}$$

and

$$P_{el}^{app} = \frac{1}{2}\hat{U}^2 \left|\tilde{Y}\right|, \tag{61}$$

respectively, where $\hat{U}$ is the amplitude of the driving voltage and $\tilde{Y}$ is the admittance of the resonator. It should be noted that the resonator performance numbers according to equations (57) and (58) are dimensionless quantities, but are not normalized to 1, in contrast to common efficiency definitions. They are functions of the ratio of the averaged stored energy in the liquid layer and the electrical energy supplied per oscillation period. Since both the numerator and denominator in (57) and (58) are proportional to the square of the voltage amplitude, the performance numbers are independent of the driving voltage. The electrical input power must be equal to the total power flow through the resonator boundary surface at $x = x_0$ (outer surface of the piezoceramic) and can therefore also be obtained from the Poynting vector:

$$P_{el}^{true} = A \cdot \Re\left\{\tilde{\Pi}(x_0)\right\}, \tag{62}$$

$$P_{el}^{app} = A\left|\tilde{\Pi}(x_0)\right|. \tag{63}$$

This follows from the fact that there is no mechanical power supplied by any sources and from the chosen potentials $\Re\{\tilde{\varphi}_1\} = \hat{U}$, $\tilde{\varphi}_2 = 0$. An additional quantity of practical interest is the total power loss in each layer that can be calculated from the power loss density given by equation (55) as:

$$\left\langle P_n^{loss} \right\rangle = A \int_{x=x_{n-1}}^{x=x_n} \left\langle \bar{P}^{loss}(x) \right\rangle dx, \tag{64}$$

where the subscript n denotes the considered layer. The total power loss within a certain layer must be equal to the difference of true energy flow at the boundary surfaces of that layer. Hence, the total power loss within a layer can also be calculated directly from the values of the Poynting vector at the layer boundaries:

$$\left\langle P_n^{loss} \right\rangle = A \left[\Re \left\{ \tilde{\Pi}(x_{n-1}) \right\} - \Re \left\{ \tilde{\Pi}(x_n) \right\} \right]. \qquad (65)$$

This approach requires much less computational effort than equation (64), since evaluation has to be carried out only for two x-values. In case of low losses ($Q_n \gg 1$), the quality factor Q_n of layer n establishes the relationship between stored energy and power loss within that layer:

$$Q_n = \omega \frac{\left\langle E_n \right\rangle}{\left\langle P_n^{loss} \right\rangle}. \qquad (66)$$

By combining equations (65) and (66), an expression for the total stored energy in the liquid layer is obtained directly:

$$\left\langle E_L \right\rangle = \frac{Q_L}{\omega} A \left[\Re \left\{ \tilde{\Pi}(x_2) \right\} - \Re \left\{ \tilde{\Pi}(x_3) \right\} \right]. \qquad (67)$$

It was shown by Burger [44] that the acoustic performance number η_{ac} of a typical resonator for ultrasonic particle separation has essentially the same frequency-dependence as the resonance sharpness (resonance quality factor) of the series resonance frequencies. The acoustic performance number is a measure of the relationship between energy density in the liquid (which is pertinent to particle separation) and the total electric input power consumption of the resonator. In general, however, the resonator does not represent a pure ohmic load (even when driven at one of its resonance frequencies). Thus, reactive power has to be provided by the source. In order to minimize the reactive power requirement, one has to choose the driving frequency with respect to maximum effective resonator performance number η_{eff}. The latter condition restricts the practical operating frequency range to a relatively narrow band, as will be shown in the next section.

4. Results and discussion

The method outlined in the previous section was applied to the analysis of a resonator chamber developed for separation of biological cells from the nutrient fluid (which has acoustic properties similar to water). Operation and performance of this device, which acts as an acoustic filter, will be described in detail in part III of this work. Herein, the discussion is focused on the electric and acoustic properties of a piezoelectric resonator with four layers, shown schematically in Figure 2. The dimensions, material constants, and parameters needed for calculation are listed in Table I in the appendix. Figure 4 shows the measured (a) and calculated (b) spectra of electrical admittance in the range from 1.8 to 2.8 MHz. For measurement, the resonator chamber was filled with degassed water. The measurement set-up is described in

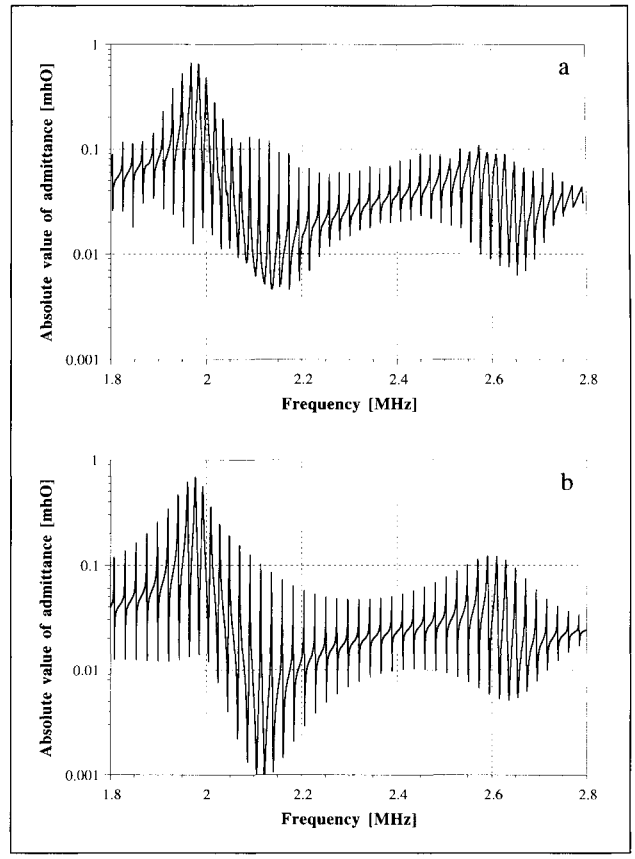

Figure 4. Spectrum of electrical admittance of the 4-layer piezoelectric resonator according to Figure 2. (a) measured, (b) calculated.

[45]. The large number of overtone resonances arises from the fact that the sound wavelength in the liquid layer is much smaller than the layer thickness. The envelope curve shows two maxima at frequencies of about 2 MHz and 2.6 MHz, respectively. These frequencies are the eigenfrequencies (series resonances) of the piezoceramic/glass composite. The lower eigenfrequency of the composite coincides with the fundamental series resonance frequency of the piezoceramic alone. This follows from the chosen layer dimensions but is not a prerequisite for efficient resonator design, as will be discussed in part II of this work. The comparison of measured and calculated admittance data shows excellent agreement. The discrepancy between the measured and calculated curves in the lower parts of Figures 4a and 4b, respectively, is due to a reduced accuracy of the measurement system in the low admittance (high impedance) range. This is caused by two facts: (1) The test object (resonator) is inserted into a low-ohmic resistance bridge, which provides best accuracy in the vicinity of the series resonance frequencies (high admittance), but less accuracy in the range of the parallel resonances (low admittance). (2) To reduce measurement time, the frequency sweep procedure is also optimized for best resolution at the series resonances, whereas the parallel resonances are skipped.

The calculated acoustic and effective resonator performance numbers are plotted as functions of frequency in Figures 5 and 6. Apart from the strong, more or less pe-

ACUSTICA · acta acustica
Vol. 84 (1998)

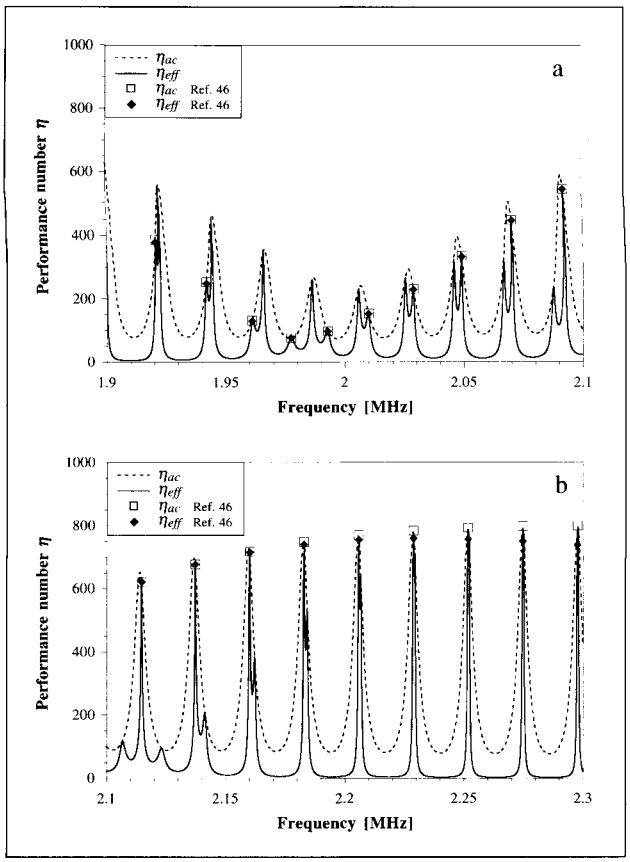

Figure 5. Calculated spectra of acoustic and effective performance numbers of the resonator according to Figure 2. For comparison, values obtained from perturbation theory [46] are also shown. (a) in the frequency range 1.9 to 2.1 MHz containing the third harmonic of the ceramic/glass-composite (approx. 2 MHz), (b) in the range between transducer-eigenfrequencies. The effective quality factor of the liquid layer was set to 6000.

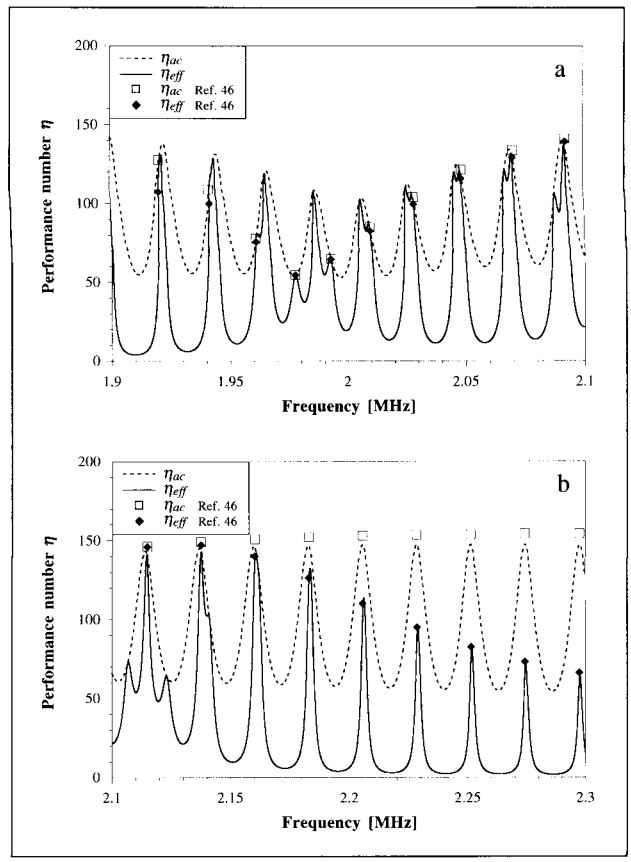

Figure 6. As Figure 5, with an effective quality factor of the liquid layer of 1000.

riodic, variation due to the large number of overtone resonances, it is remarkable that the performance number reaches a maximum in the range between the eigenfrequencies of the transducer, while it drops down in the range close to the eigenfrequencies. The full and dashed lines show the results obtained from calculations using equations (57) and (58), respectively. For comparison, values obtained by a different treatment based on perturbation theory [46] are also plotted. Within that model the performance numbers can be calculated only at the series resonances. Hence, the black and white dots in Figures 5 and 6 also mark the series resonance frequencies. In Figure 5 the acoustic material quality factor of the liquid Q_L was set to 6000, corresponding to the measured effective quality factor of degassed water. In this case, the high-performance range is rather broad and covers a number of resonances. During practical operation of the cell filter, a decrease of the quality factor with increasing cell concentration in the suspension is experienced. Figure 6 shows the corresponding results for $Q_L = 1000$, which corresponds to a typical effective acoustic quality factor of a high-density cell suspension. Besides the performance number decrease due to the higher losses in the liquid, a significant narrowing of the optimal frequency range is seen (compare Figures 5b and 6b). This effect has been observed in separation processes of high-density cell cultures [47]. The reduction of the effective performance number is mainly caused by a decrease of the electric power factor (i.e. an increase of the phase shift between voltage and current). Another interesting fact is that the frequencies of relative performance number maxima coincide well with the series resonance frequencies in the range between the eigenfrequencies of the transducer, while this is not the case in the region close to the eigenfrequencies. In case of varying properties of the suspension during the separation process (increasing particle concentration, decreasing quality factor Q_L), one has to choose the driving frequency according to a compromise between optimum performance at high- and low-Q conditions. Based on this consideration, the resonance frequency of 2.16 MHz can be regarded as an optimal operating frequency for the resonator discussed here. It should be noted that for a homogeneous resonator the acoustic performance number η_{ac} is independent of frequency. The strong variation with frequency, as shown here, is a consequence of the frequency-dependent energy distribution among the layers of the multilayered structure. In contrast, η_{eff} depends on frequency even for a single-layer resonator, since it is influenced by the electric phase angle (power factor).

In Figure 7 the spatial distribution of displacement velocity, energy flow, energy density and power loss density in the resonator, calculated for the optimal frequency of 2.16 MHz,

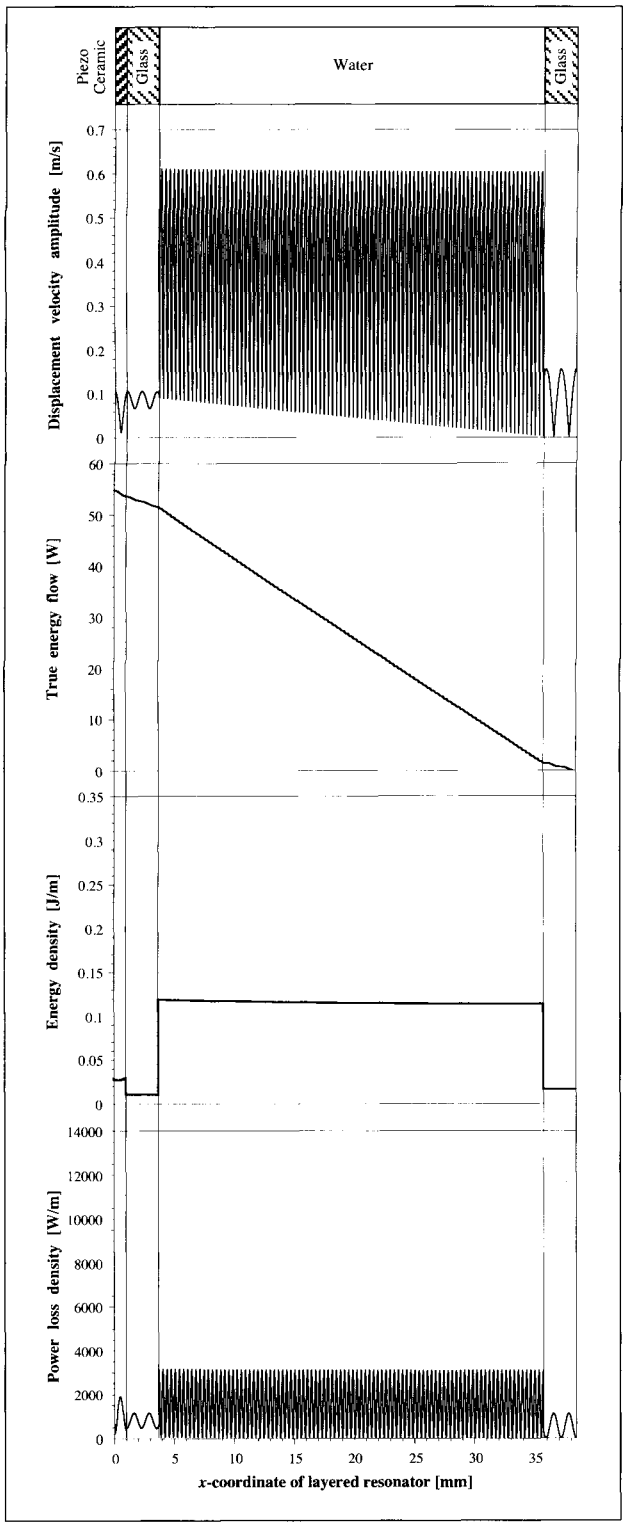

Figure 7. Spatial distribution of displacement velocity amplitude, true energy flow, energy density and power loss density within the layers of the resonator according to Figure 2; calculated for the series resonance frequency of 2.16 MHz. The apparent electric input power was supposed to be 60 VA, the effective quality factor of the liquid was set to 1000.

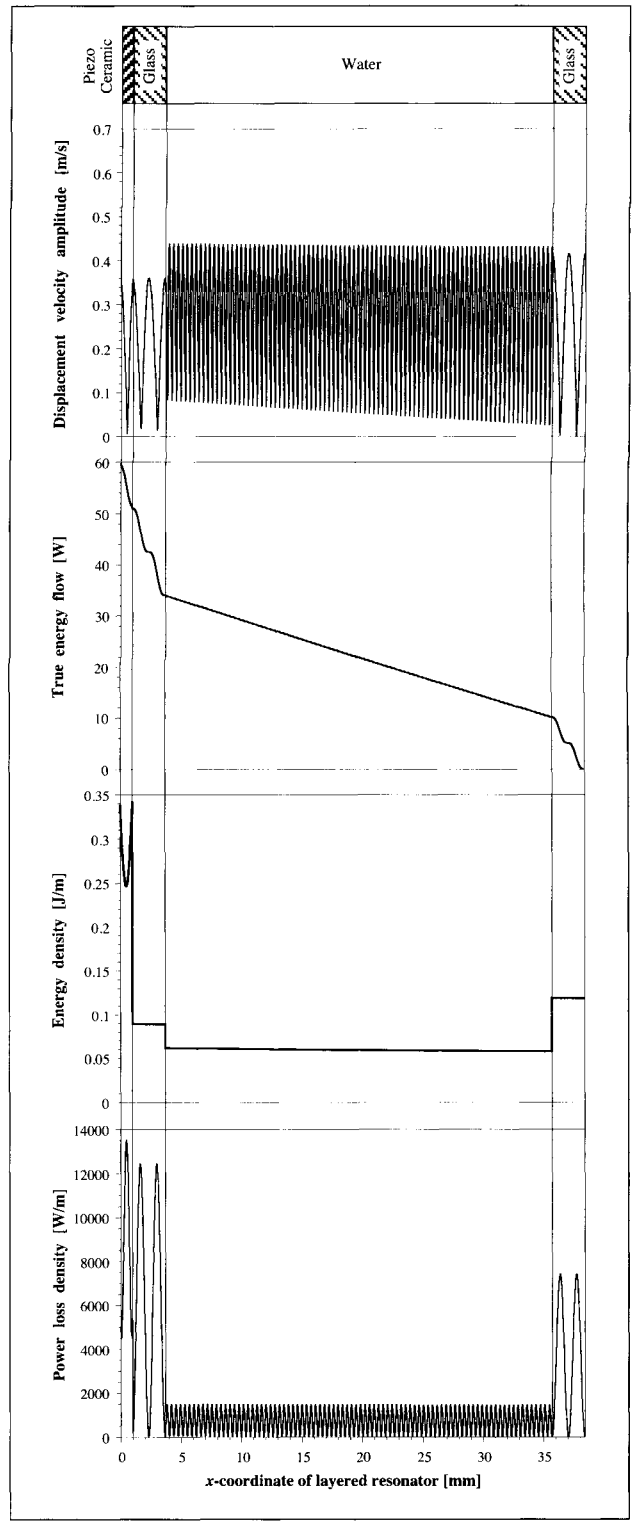

Figure 8. As Figure 7, calculation was carried out for the resonance frequency of 1.99 MHz.

is plotted. The displacement velocity amplitude obtained by taking the absolute value of the velocity according to equation (52) shows the characteristics of a quasi-standing wave (compare to Figure 1). The total true energy flow is calculated from the real part of equation (53), multiplied by the cross-sectional area A of the resonator. The (one-dimensional) density of stored energy is given by equation (54) after multiplication with the area A. The (one-dimensional) power loss density is obtained from equation (55) by multiplication with

ACUSTICA · acta acustica
Vol. 84 (1998)

A. An electric input power of 60 VA (apparent power), which is a typical value for the considered resonator, was assumed for these calculations. The quality factor of the liquid was set to $Q_L = 1000$. A significant rise of velocity amplitude, as well as of energy density, in the liquid layer, compared to the transducer, is found. This corresponds to the maximum performance number (maximum resonator efficiency) occurring at the frequency considered. In contrast, Figure 8 shows the situation at a series resonance frequency of 1.99 MHz, which is close to the eigenfrequency of the transducer. In this case, the velocity amplitudes are nearly equal in all layers. The energy density is lowest in the liquid and the power loss densities are extremely high in the piezoceramic and the carrier. With equal electric power supplied, the energy density in the liquid is about twice as high in the first case (Figure 7), although the utilized true power is about 8% less due to a higher reactive power component.

The increased displacement velocity amplitude in the liquid compared to the transducer, when the resonator is operated between the eigenfrequencies of the transducer, can be explained as follows: The displacement (or velocity) amplitude in the liquid layer depends not only on the displacement at the boundary surface between transducer and liquid, but also on the stress amplitude at this surface, as is evident from equation (33). At the eigenfrequencies of the transducer, the stress amplitude at that boundary surface vanishes (i.e. the boundary condition $T = 0$, which generally applies to the free surfaces of the layered resonator, is transferred to the inner boundary surface). At other frequencies, both displacement and stress at the inner boundary layer can reach significant values. Provided the resonance sharpness of the eigenfrequencies of the transducer is low (which is generally the case for the considered transducers), overtone resonances of the layered structure are excitable between these eigenfrequencies and the displacement velocity as well as the energy density in the liquid are higher at those resonances. The absolute values of resonance frequencies with high or low efficiency (performance numbers) are of course dependent on the resonator structure. In particular, different thicknesses of the glass carrier lead to different eigenfrequencies. However, the qualitative behaviour of the resonator remains unchanged, i.e. resonances with highest efficiency again occur in the range between the eigenfrequencies.

To estimate the allowable input power, knowledge of the power loss distribution in the resonator is essential. The calculated loss distribution among the four layers is shown in Figures 9a and 9b. In the frequency range between the eigenfrequencies of the transducer (Figure 9b), the series resonance frequencies coincide with maximum power loss (due to maximum velocity amplitude) in the liquid and minimum power loss in the piezoceramic and the carrier. Close to the eigenfrequencies of the transducer, in general, the series resonances do not correspond to minima or maxima of power loss and stored energy in any layer (Figure 9a). The high losses in the glass reflector around 2 MHz are due to an eigenresonance of the reflector plate in that frequency range.

Finally, to verify the validity of the applied model, the following experiment was carried out: The resonator was filled

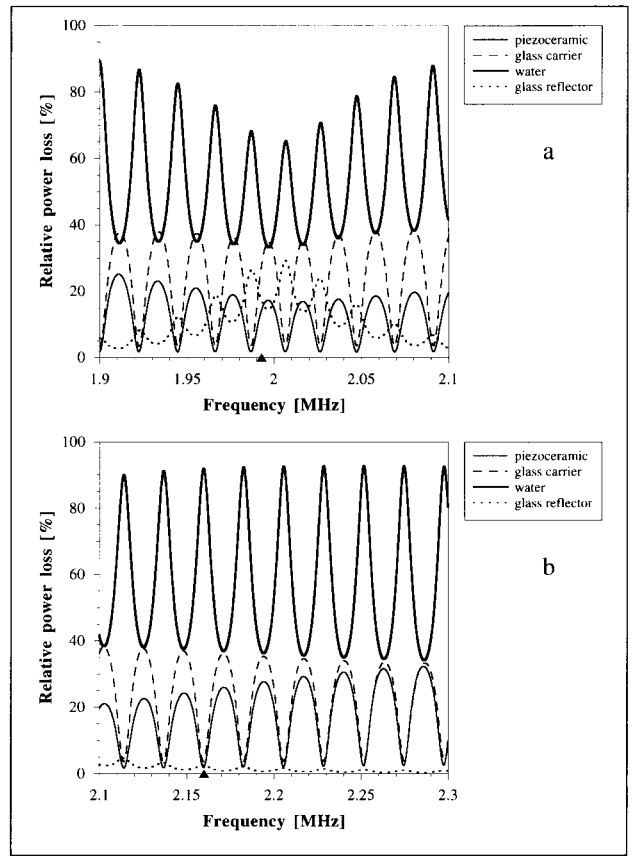

Figure 9. Calculated power loss distribution among the layers of the resonator according to Figure 2. (a) within the range of an eigenfrequency of the transducer, (b) in the range between transducer-eigenfrequencies. The series resonance frequencies of 1.99 MHz and 2.16 MHz, respectively, are marked on the frequency-axis. The effective quality factor of the liquid was set to 1000.

with a low-concentrated suspension of corundum powder in water ($a = 2.5\,\mu$m, $\lambda = 3.7$, $\sigma = 2.45$) and driven at a resonance frequency of 2.205 MHz. The set-up was arranged with the direction of sound propagation oriented vertically. Due to the acoustic radiation force, the particles formed planes perpendicular to the sound propagation direction. After steady-state conditions were established, the driving voltage of the transducer was slowly reduced until particle sedimentation due to gravity was observed. The onset of this effect was found at a voltage amplitude of 18 V. The gravitational force minus the buoyancy force acting on the particles is $F = g(\rho_0 - \rho)V = 1.7 \cdot 10^{-12}$ N. For a driving voltage amplitude of 1 V and a measured effective quality factor of the suspension of 2500, one obtains from equation (56) an energy density in the liquid layer of $\langle \bar{E} \rangle = 8 \cdot 10^{-3}$ J/m^3. With this value and the acoustic contrast factor of $K = 0.64$, the amplitude of the radiation force calculated from equation (2) is $\langle \hat{F}_s \rangle = 9 \cdot 10^{-15}$ N. This yields a minimum voltage amplitude for retaining the particles against gravity of approximately 14 V. This calculated result is in good agreement with the experimental threshold value of 18 V, since settling of the particles begins rather smoothly than at a well-defined voltage level. Nevertheless,

the discrepancy can be attributed to an over-estimation of the energy density in the liquid. This is mainly due to the non-ideal behaviour of the resonator (striated columns of particles were observed rather than uniform planes) and because the electronic frequency control may not have maintained the resonance condition precisely at such low power levels.

5. Conclusion

A mathematical description of layered piezoelectric resonators has been presented, with special emphasis on resonators for ultrasonic separation of suspensions or emulsions. The model is a powerful tool for the proper design of separation chambers, the determination of optimum operating frequency ranges, and the calculation of energy input to the suspension. With knowledge of the energy density, the acoustic radiation force acting on suspended particles could be calculated. Given a suspension with known properties, the total power input to the resonator required for a certain mean energy density in the suspension can be estimated.

The one-dimensional model allows relatively simple computations and shows very good agreement with experiments. The reason for the validity of the one-dimensional treatment in describing the non-ideal layered resonator is, that all effects not contributing to the generation of one-dimensional standing waves can be considered as losses and described in a global way by effective acoustic quality factors Q_{eff} for each layer. These factors can be determined by fitting calculated to measured spectra of electrical admittance. Q_{eff} of the piezoceramic is obtained from the measured resonance quality factor (resonance sharpness) of the eigenmode considered. The quality factors of the carrier and reflector materials can be taken from literature, whereby the damping effect of the glueing layer between piezoceramic and carrier can be accounted for by a reduced Q_{eff} of the carrier. This can be proven experimentally by measuring the resonance sharpness of the composite transducer. Finally, the effective quality factor of the liquid has to be determined from the admittance spectrum of the whole resonator. Thereby, the sharpness of resonances in the range between the eigenfrequencies of the transducer gives a good measure for Q_{eff} of the liquid. This is a consequence of the fact, that the electrical properties of the layered resonator are strongly influenced by the properties of the liquid in this frequency range, whereas close to the eigenfrequencies of the transducer, the influence of the piezoceramic layer and the carrier layer is dominating. This behaviour is typical for layered resonators with a liquid layer much thicker than the other layers. All other parameters needed for calculations by means of the discussed model are usually specified by the manufacturer of the piezoceramic or well known from literature.

When driving a resonator for particle separation, a significant temperature dependence of the resonance frequencies is observed. This is mainly due to the temperature dependence of the sound speed in the liquid, which causes a typical resonance frequency shift in the range of 2 to 3 kHz/°C. Comparison of this value with the resonance bandwidth, which is normally less than 2 kHz, shows clearly the necessity of an automatic resonance control. Means of frequency control as well as other aspects related to the design and practical operation of separation devices, such as resonator geometry and material selection, the principle of a high-efficiency driving source and limitations to power input, will be discussed in part II of this work.

Acknowledgement

The author would like to gratefully acknowledge the many valuable discussions with E. Benes, W. Burger, H. Nowotny and F. Trampler from the University of Technology, Vienna, Austria. This work has been supported by the Austrian "Forschungsförderungsfonds für die gewerbliche Wirtschaft", Project Nos. 5/652, 6/724, and 6/772, and by Anton PAAR GmbH, Graz, Austria.

Appendix

Parameters for calculation

The results presented in section 4 were obtained with the data set given in Table I. The material parameters ρ, ν, κ, ε, and $\tan\vartheta$, of the piezoceramic and glass, respectively, are specified by the manufacturer. The effective acoustic quality factors Q_{eff} were determined from measured admittance spectra. For completeness, the fundamental constants $c = \rho\nu^2(1-\kappa^2)$, and $e = \kappa\nu\sqrt{\rho\varepsilon}$, are also listed. According to the one-dimensional model used, all quantities are reduced to scalars and apply in the direction of sound propagation (thickness direction of piezoceramic and glass plates, respectively).

The transducer of the considered resonator consists of two piezoceramic square (25×25 mm) discs, glued on the glass carrier and electrically connected in series. The total cross-sectional area A of the sonicated volume is $1.25 \cdot 10^{-3}$ m^2.

List of symbols

a radius of suspended spherical particle [m]
A cross-sectional area of layered resonator [m^2]
c elastic stiffness constant [Pa = Nm^{-2}]
$\bar{c}$ piezoelectrically stiffened elastic constant [Pa]
d center-to-center distance between two suspended particles [m]
D dielectric displacement [Cm^{-2}=Asm^{-2}=NV^{-1}m^{-1}]
e piezoelectric constant [Cm^{-2}]
E energy [J = Nm]
$\bar{E}$ energy density [Jm^{-3}]
F force [N]
g acceleration due to gravity [ms^{-2}]
$\mathrm{j} = \sqrt{-1}$ imaginary unit [–]
$k = \omega/\nu$ wave number [m^{-1}]
$k_0 = \omega/\nu_0$ wave number of the longitudinal acoustic wave

ACUSTICA · acta acustica
Vol. 84 (1998)

Table I. Parameters and material constants of the 4-layer piezoelectric resonator.

	Piezoelectric Layer	Carrier Layer	Liquid Layer	Reflector Layer
Material (Manufacturer)	Sonox P4 (Hoechst, Germany)	Tempax glass (Schott, Germany)	Degassed water	Tempax glass (Schott, Germany)
Thickness ℓ [mm]	1.01	2.71	32	2.71
Density ρ [kg/m^3]	7800	2200	998	2200
Sound speed ν [m/s]	4460	5430	1485	5430
Electromech. coupling factor κ	0.5	–	–	–
Dielectric constant ε [As/Vm]	$6.02 \cdot 10^{-9}$	–	–	–
Tangent of loss angle $\tan\vartheta$	0.007	–	–	–
Effective acoustic quality factor Q_{eff}	400	180	6000/1000	400
Elastic stiffness constant c [GPa]	116	64.9	2.2	64.9
Piezoelectric constant e [N/Vm]	15.3	–	–	–

in the particle material [m^{-1}]
K acoustic contrast factor [–]
ℓ layer thickness in direction of sound propagation [m]
p acoustic pressure [Pa]
P power [W]
$\bar{P}$ power density [Wm^{-3}]
P_{el}^{app} electric apparent power [W]
P_{el}^{true} electric true power [W]
Q acoustic material quality factor [–]
R reflection coefficient [–]
S strain [m/m = 1]
t time [s]
T stress [Pa]
u displacement of the sound wave [m]
U resonator driving voltage [V]
$v = \partial u/\partial t$ displacement velocity of the sound wave [ms^{-1}]
V volume of suspended particle [m^3]
x space coordinate in direction of sound propagation [m]
Y electrical admittance [Ω^{-1}]
α linear (amplitude) absorption coefficient [m^{-1}]
β compressibility [Pa^{-1} = m^{2}N^{-1}]
δ penetration depth of viscous wave [m]
ε dielectric constant [Fm^{-1} = AsV^{-1}m^{-1}]
ϕ radiation force potential [Nm]
γ electric conductivity [Ω^{-1}m^{-1}]
η resonator performance number [–]
ϑ dielectric loss angle [rad]
φ electric potential [V]
Φ velocity potential of the sound wave [m^{2}s^{-1}]
κ electromechanical coupling factor [–]
λ ratio of mass densities (see below) [–]
μ shear viscosity [kgm^{-1}s^{-1}]
μ' bulk viscosity [kgm^{-1}s^{-1}]
$\nu = \omega/k$ speed of sound [ms^{-1}]
$\nu_0 = \omega/k_0$ sound speed of the longitudinal acoustic wave in the particle material [ms^{-1}]
Π Poynting vector (energy flow density) [Wm^{-2}]
θ angle between centerline of two particles and direction of sound propagation [rad]
ρ mass density [kgm^{-3}]
ρ_0 mass density of suspended particle [kgm^{-3}]
σ sound speed ratio (see below) [–]
ω angular frequency [s^{-1}]

Subscripts and superscripts

0 suspended particle
ac acoustic performance number
eff effective quality factor, absorption coefficient or performance number, respectively
kin kinetic energy density
n number of resonator layer
p progressive wave
pot potential energy density
qs quasi-standing wave
s standing wave
vis viscous case
C carrier layer
E electrode
L liquid layer
P piezoelectric layer
R reflector

Time-averaged quantities are denoted by angle brackets: $\langle\ \rangle$. Complex quantities are marked by the tilde-sign:˜. The symbol ˆ denotes amplitudes (which are real, positive constants) of quantities with harmonic time- and space-dependence. The following ratios are defined for abbreviation: $\lambda = \rho_0/\rho$, $\sigma = \nu_0/\nu = k/k_0$, whereby ρ_0, ν_0, k_0, refer to the suspended particle and ρ, ν, k, refer to the host fluid.

References

[1] R. E. Apfel: Acoustic radiation pressure - principles and application to separation science. Fortschritte der Akustik - DAGA '90. DPG-GmbH, Bad Honnef, Germany, 1990. 19–36. Teil A. ISBN 3-923835-07-8.
[2] C. J. Schram: Manipulation of particles in an acoustic field. – In: Advances in Sonochemistry. Vol. 2. T. J. Mason (ed.). JAI Press Ltd., London, 1991, 293–322.

[3] W. T. Coakley, G. Whitworth, M. A. Grundy, R. K. Gould, R. Allman: Ultrasonic manipulation of particles and cells. Bioseparation **4** (1994) 73–83.
[4] F. Trampler, S. A. Sonderhoff, P. W. S. Pui, D. G. Kilburn, J. M. Piret: Acoustic cell filter for high density perfusion culture of hybridoma cells. Bio/Technology **12(3)** (1994) 281–284.
[5] O. Doblhoff-Dier, T. Gaida, H. Katinger, W. Burger, M. Gröschl, E. Benes: A novel ultrasonic resonance field device for the retention of animal cells. Biotechnol. Prog. **10(4)** (1994) 428–432.
[6] L. D. Landau, E. M. Lifshitz: Fluid mechanics. Pergamon, New York, 1959.
[7] L. V. King: On the acoustic radiation pressure on spheres. Proc. R. Soc. London **A147** (1934) 212–240.
[8] K. Yosioka, Y. Kawasima: Acoustic radiation pressure on a compressible sphere. Acustica **5** (1955) 167–173.
[9] S. D. Danilov, M. A. Mironov: Radiation pressure force acting on a small particle in a sound field. Sov. Phys. Acoust. **30(4)** (1984) 280–283.
[10] L. P. Gor'kov: On the forces acting on a small particle in an acoustical field in an ideal fluid. Sov. Phys. Dokl. **6(9)** (1962) 773–775.
[11] W. L. Nyborg: Radiation pressure on a small rigid sphere. J. Acoust. Soc. Am. **42(5)** (1967) 947–952.
[12] L. A. Crum: Acoustic force on a liquid droplet in an acoustic stationary wave. J. Acoust. Soc. Am. **50(1)** (1971) 157–163.
[13] W. König: Hydrodynamisch-akustische Untersuchungen: II. Über die Kräfte zwischen zwei Kugeln in einer schwingenden Flüssigkeit und über die Entstehung der Kundt'schen Staubfiguren. Ann. Phys. Chem. **42(4)** (1891) 549–563.
[14] V. F. K. Bjerknes: Die Kraftfelder. Vieweg und Sohn, Braunschweig, Germany, 1909.
[15] L. A. Crum: Bjerknes forces on bubbles in a stationary sound field. J. Acoust. Soc. Am. **57(6)** (1975) 1363–1370.
[16] N. Pelekasis, J. Tsamopoulos: Bjerknes forces between 2 bubbles. Part I: Response to a step change in pressure. J. Fluid Mech. **254** (1993) 467–499.
[17] N. Pelekasis, J. Tsamopoulos: Bjerknes forces between 2 bubbles. Part II: Response to an oscillatory pressure field. J. Fluid Mech. **254** (1993) 501–527.
[18] X. Zheng, R. E. Apfel: Acoustic interaction forces between two fluid spheres in an acoustic field. J. Acoust. Soc. Am. **97(4)** (1995) 2218–2226.
[19] M. A. H. Weiser, R. E. Apfel: Interparticle forces on red cells in a standing wave field. Acustica **56** (1984) 114–119.
[20] P. J. Westervelt: The theory of steady forces caused by sound waves. J. Acoust. Soc. Am. **23(4)** (1951) 312–315.
[21] A. A. Doinikov: Acoustic radiation pressure on a rigid sphere in a viscous fluid. Proc. R. Soc. London **A447** (1994) 447–466.
[22] A. A. Doinikov: Acoustic radiation pressure on a compressible sphere in a viscous fluid. J. Fluid Mech. **267** (1994) 1–21.
[23] J. Lighthill: Acoustic streaming. J. Sound Vib. **61(3)** (1978) 391–418.
[24] F. Hager: Nonlinear and viscous effects in acoustic separation processes. Dissertation. University of Technology, Vienna, Austria, 1991.
[25] T. Hasegawa, Y. Watanabe: Acoustic radiation pressure on an absorbing sphere. J. Acoust. Soc. Am. **63(6)** (1978) 1733–1737.
[26] V. A. Sutilov: Fundamental physics of ultrasound. Gordon and Breach Science Publ., New York, 1988.
[27] B. A. Auld: Acoustic fields and waves in solids. Vol. 1. John Wiley and Sons, New York, 1973.
[28] T. Hasegawa: Acoustic radiation force on a sphere in a quasistationary wave field - theory. J. Acoust. Soc. Am. **65(1)** (1979) 32–40.
[29] E. Benes, F. Hager, W. Stuckart, H. Frischherz: Abscheidung dispergierter Teilchen durch Ultraschall-induzierte Koagulation. Fortschritte der Akustik - DAGA '89. DPG-GmbH, Bad Honnef, Germany, 1989. 255–258. ISBN 3-923835-06-X.
[30] G. Whitworth, W. T. Coakley: Particle column formation in a stationary ultrasonic field. J. Acoust. Soc. Am. **91(1)** (1992) 79–85.
[31] K. S. Van Dyke: The electric network equivalent of a piezoelectric resonator. Phys. Rev. **25** (1925) 895.
[32] E. Hafner: Resonator and device measurements. – In: Precision Frequency Control. Vol. 2. E. A. Gerber, A. Ballato (eds.). Academic, Orlando, FL, USA, 1985, 1–44.
[33] A. Ballato, H. L. Bertoni, T. Tamir: Systematic design of stacked-crystal filters by microwave network methods. IEEE Trans. Microwave Theory Tech. **22(1)** (1974) 14–25.
[34] J.-L. Dion: New transmission line analogy applied to single and multilayered piezoelectric transducers. IEEE Trans. Ultrason., Ferroelec., Freq. Contr. **40(5)** (1993) 577–583.
[35] E. L. Adler: Matrix methods applied to acoustic waves in multilayers. IEEE Trans. Ultrason., Ferroelec., Freq. Contr. **37(6)** (1990) 485–490.
[36] J. T. Stewart, Y.-K. Yong: Exact analysis of the propagation of acoustic waves in multilayered anisotropic piezoelectric plates. IEEE Trans. Ultrason., Ferroelec., Freq. Contr. **41(3)** (1994) 375–390.
[37] M. J. S. Lowe: Matrix techniques for modeling ultrasonic waves in multilayered media. IEEE Trans. Ultrason., Ferroelec., Freq. Contr. **42(4)** (1995) 525–542.
[38] H. Nowotny, E. Benes: General one-dimensional treatment of the layered piezoelectric resonator with two electrodes. J. Acoust. Soc. Am. **82(2)** (1987) 513–521.
[39] M. Schmid, E. Benes, W. Burger, V. Kravchenko: Motional capacitance of layered piezoelectric thickness-mode resonators. IEEE Trans. Ultrason., Ferroelec., Freq. Contr. **38(3)** (1991) 199–206.
[40] IEEE standard on piezoelectricity, No. 176. 1978.
[41] H. Nowotny, E. Benes, M. Schmid: Layered piezoelectric resonators with an arbitrary number of electrodes (general one-dimensional treatment). J. Acoust. Soc. Am. **90(3)** (1991) 1238–1245.
[42] R. Holland: Representation of dielectric, elastic, and piezoelectric losses by complex coefficients. IEEE Trans. Sonics Ultrason. **14(1)** (1967) 18–20.
[43] R. Holland, E. P. EerNisse: Design of resonant piezoelectric devices. Research monograph No. 56. M.I.T. Press, Cambridge, Mass., USA, 1969.
[44] W. Burger, M. Gröschl, F. Trampler, E. Benes: Frequency dependence of the acoustic loss distribution in piezoceramic/liquid resonators. Ultrasonics International '93, Conference Proceedings, Butterworth-Heinemann, Oxford, UK, 1993. 507–510. ISBN 0 750618 779.
[45] M. Schmid, E. Benes, R. Sedlaczek: A computer-controlled system for the measurement of complete admittance spectra of piezoelectric resonators. Meas. Sci. Technol. **1** (1990) 970–975.
[46] W. Burger: Anwendung von Ultraschallresonanzfeldern zur Zellrückhaltung und -abscheidung in der Biotechnologie. Dissertation. University of Technology, Vienna, Austria, 1994.
[47] S. A. Sonderhoff: SonoSep Biotech Inc., Vancouver, Canada. Personal communication.